The Rate of P-Glycoprotein Activation Depends on the Metabolic State of the Cell †

ARTICLE *in* BIOCHEMISTRY · DECEMBER 2004

Impact Factor: 3.02 · DOI: 10.1021/bi048761s · Source: PubMed

3 AUTHORS, INCLUDING:

Ewa Gatlik
Novartis
6 PUBLICATIONS **191** CITATIONS
SEE PROFILE

Anna Seelig
University of Basel
79 PUBLICATIONS **5,614** CITATIONS
SEE PROFILE

The Rate of P-Glycoprotein Activation Depends on the Metabolic State of the Cell†

Ewa Gatlik-Landwojtowicz, Päivi Äänismaa, and Anna Seelig*

Biophysical Chemistry, Biozentrum, University of Basel, Klingelbergstrasse 70, CH-4056 Basel, Switzerland

Received June 15, 2004; Revised Manuscript Received September 7, 2004

ABSTRACT: P-glycoprotein ATPase activity has been studied almost exclusively by measuring inorganic phosphate release from inside-out cellular vesicles. We have recently proposed a new method based on measurements of the extracellular acidification rate (ECAR) of living cells with a Cytosensor microphysiometer. This method allows for systematic investigation of the various factors influencing P-glycoprotein activation in living cells. Basal metabolic rates or ECARs of different *MDR1*-transfected cell lines were compared with those of the *Mdr1a*$^{-/-}$*1b*$^{-/-}$ knockout, *MRP1*-transfected, and corresponding wild-type cell lines. Basal ECARs of all cells were on the order of 10^7 protons/cell/s, whereby those of genetically modified cells were on average (over all cell lines) slightly lower than those of wild-type cells. The expression level of P-glycoprotein in *MDR1*-transfected cells had no influence on basal ECARs. Verapamil-induced ECARs were specific for *MDR1*-transfected cells and increased with the expression level of P-glycoprotein. Moreover, ECARs were dependent on the metabolic state of the cell and were $(2.8 \pm 1.2) \times 10^6$ and $(8.0 \pm 1.5) \times 10^6$ protons/cell/s in glucose-deficient and glucose-fed NIH-MDR-G185 cells, respectively, after verapamil (10 μM) stimulation. The ECARs were practically identical to the rates of lactate extrusion and thus reflect the rates of ATP synthesis via glycolysis. Taking into account the number of P-glycoprotein molecules per cell, the rate of ATP hydrolysis in inside-out vesicles of the same cells was determined as $(9.2 \pm 1.5) \times 10^6$ phosphates/cell/s, in good agreement with the rate of ATP synthesized in glucose-fed cells. The energy required for P-glycoprotein activation *relative* to the basal metabolic energy was twice as large in glucose-deficient as in glucose-fed cells, suggesting cellular protection by P-glycoprotein even under conditions of starvation.

P-glycoprotein (Pgp),[1] a product of the multidrug resistance gene, *MDR1*, is an efflux transporter with broad substrate specificity. It binds a large variety of exogenous and endogenous toxic compounds within the plasma membrane and exports them to the extracellular environment (*1*−*3*). Transport of substrates by Pgp out of the cell is driven by metabolic energy. Per substrate transported one to two (or even three) molecules of ATP are hydrolyzed (*4*−*8*). The first molecule is proposed to drive drug transport and the second to reset the conformation of the transporter (*7*). However, even in the absence of exogenous substrates Pgp shows basal ATPase activity in plasma membrane vesicles (*9*−*11*) as well as in proteoliposomes (*12*, *13*). Basal Pgp activity was suggested to arise either from transport of endogenous lipids (*14*, *15*) or from uncoupled ATPase activity (*16*, *17*).

Pgp activation can be measured with reconstituted proteoliposomes or inside-out membrane vesicles of *MDR1*-transfected cells by monitoring ATP hydrolysis via either inorganic phosphate release (*8*, *9*, *13*) or ADP formation (*10*, *18*).

In intact *MDR1*-transfected cells Pgp activation can be analyzed noninvasively via extracellular proton secretion. As demonstrated, extracellular acidification rates, ECARs, of living cells can be quantified with a silicon-based potentiometric sensor (Cytosensor microphysiometer) (*19*), and the first systematic measurement of the effect of drugs on living *MDR1*-transfected cells has been published recently (*20*). Plots of the ECAR as a function of the logarithm of the drug concentration were bell-shaped, indicating activation at low and inhibition at high drug concentrations, and were consistent with Pgp activation/inhibition profiles measured previously by means of phosphate release measurements in inverted membrane vesicles for the same drugs (*9*). The concentrations of half-maximum activation for the different compounds investigated were practically identical for the two methods. Furthermore, a linear correlation between the rate of extracellular proton release and the intracellular phosphate release was obtained, indicating the quantitative equivalence of assays with plasma membrane vesicles and *living* cells (*20*).

Previous measurements of extracellular pH changes by conventional methods have led to conflicting results, arguing either in favor of (*21*, *22*) or against extracellular acidification (*21*, *23*). The bell-shaped activation/inhibition curves measured with the Cytosensor can partly explain these discrepancies since both activation and inhibition of extracellular acidification can be induced depending on the drug concentration employed.

† Supported by the Swiss National Science Foundation, Grant No. 31-58800.99.

* To whom correspondence should be addressed. Phone: +41-61 267 22 06. Fax: +41-61 267 21 89. E-mail: Anna.Seelig@unibas.ch.

[1] Abbreviations: ECAR, extracellular acidification rate; *MDR1*, multidrug resistance 1 gene; *MRP1*, multidrug resistance-associated protein gene; Pgp, P-glycoprotein, product of the *MDR1* gene.

10.1021/bi048761s CCC: $27.50
Published on Web 10/30/2004

Extracellular acidification reflects, in some general way, the *overall* metabolism of the cell (*24*). In contrast, the ATP hydrolysis assay involving proteoliposomes or inside-out vesicles is focused on a *single* metabolic event, analyzed without any relation to the metabolic state of the intact cell. Three general questions then emerge in this context. (i) To what extent is the metabolic activity of a living cell influenced by the expression level of Pgp? Whether Pgp overexpression influences the basal cellular metabolism is discussed controversially in the literature. Intracellular alkalization in cells overexpressing Pgp in comparison to wild-type cells has been observed by some investigators (*21*, *25*−*30*), whereas neither intracellular (*23*, *31*−*33*) nor extracellular basal pH changes were observed by others (*23*, *32*). Also no difference was found between cells overexpressing the multidrug resistance-associated protein, MRP1, and wild-type cells (*34*). (ii) How do variations of the metabolic state of the cell, such as starvation, regulate, in turn, the drug-induced activation of Pgp? ATP concentrations used in Pgp activation assays with inside-out membrane vesicles are rather high (3−7.5 mM) (*9*, *10*) since the Michaelis−Menten constant of ATP is $K_m = 0.33 \pm 0.04$ mM (*10*). In living cells, ATP concentrations are in a similar range or even higher under optimal conditions; however, they can vary with the metabolic state of the cell. Moreover, ATP has to be shared by different energy-dependent proteins. It is therefore of interest to test how the process of cellular detoxification by Pgp changes with the metabolic state of the cell. (iii) How is the general mechanism of extracellular acidification, under conditions of Pgp activation, linked to the specific process of Pgp-induced ATP hydrolysis?

The aim of the present work is therefore (i) to clarify the influence of the expression level of Pgp on basal metabolism, (ii) to measure the basal and verapamil-induced ECARs in living, *MDR1*-transfected cells under different metabolic conditions by means of a Cytosensor, (iii) to identify the export pathways of the acidic metabolites, and (iv) to compare the different ECARs obtained in living cells with the rate of Pgp ATP hydrolysis in inside-out vesicles of the same cells. Basal and verapamil-stimulated ECARs were assessed for different *MDR1*-transfected cell lines (*MDR1*-transfected pig kidney cells LLC-MDR1 (*35*), mouse embryo fibroblasts NIH-MDR-G185 (*36*)), for three other genetically modified cell lines (LLC-PK1 transfected with the human *MRP1* gene (*37*), cells 77.1 and 88.6, lacking functional Pgp, obtained from Mdr1a$^{-/-}$1b$^{-/-}$ mouse embryos (*38*)), and for the corresponding wild-type cell lines. In addition, special attention was given to the number of passages the various cell types had experienced since this turned out to be a further parameter influencing the basal extracellular acidification rates. The experiments will provide new insight into the mechanism of Pgp activation in living cells.

MATERIALS AND METHODS

Compounds. Colchicine, phloretin, and 2-deoxy-D-glucose were obtained from Fluka (Buchs, Switzerland), 4,4′-diisothiocyanatostilbene-2,2′-disulfonic acid, DIDS, verapamil, vincristine, and sodium pyruvate from Sigma (Steinheim, Germany), and lactate reagents and lactate standard solutions (Cat. Nos. 735-10 and 826-10, respectively) from Sigma Diagnostics Inc. (St. Louis, MO). The other chemicals were from Fluka, Merck, or Sigma. Complete EDTA-free protease inhibitor cocktail tablets were obtained from Roche Diagnostics (Mannheim, Germany), 1,4-dithiol-DL-threit(ol), DTT, was from Applichem (Darmstadt, Germany), and BCA protein assay reagents were purchased from Pierce (Rockford, IL). DMEM (liquid and dry, Cat. Nos. 21969 and 52100, respectively) without pyruvate, IMDM medium, and other compounds required for cell culture such as fetal bovine serum, FBS, bovine serum albumin, BSA, and antibiotics were from Gibco-BRL (Basel, Switzerland). P-glycoprotein antibody, MRK16, and unspecific antibody, IgG_{2ak}, were from Kamiya Biomedical Co. (Seattle, WA), and the IgG_{2a} FITC-labeled antibody was from PharMingen (San Diego, CA).

Cell Lines. The mouse embryo fibroblast wild-type lines (2ac.1 and 2ac.2) and lines lacking functional Pgp (77.1 and 88.6) from Mdr1a$^{-/-}$1b$^{-/-}$ mouse embryos were generously provided by Dr. A. H. Schinkel (The Netherlands Cancer Institute, Amsterdam, The Netherlands), the pig kidney epithelial cell lines LLC-PK1, LLC-PK1 transfected with the human *MDR1* gene (LLC-MDR1), and LLC-PK1 transfected with the human *MRP1* gene (LLC-MRP1) by Dr. P. Borst (The Netherlands Cancer Institute), and the mouse embryo fibroblast lines NIH3T3 and NIH3T3 transfected with the human *MDR1* gene (NIH-MDR-G185) by Dr. M. M. Gottesman (The National Institutes of Health, Bethesda, MD).

Cell Culture. All cell lines were grown under the same conditions in monolayer culture in DMEM medium (4.5 g/L glucose) supplemented with fetal bovine serum (10% v/v), penicillin (100 units/mL), streptomycin (100 μg/mL) and L-glutamine (146 mg/L) at 37 °C in an atmosphere containing CO_2 (5%). NIH-MDR-G185 and LLC-MDR1/V cells were grown in the presence of colchicine (0.15 μM) and vincristine, V (0.32 μM), respectively. The cells were passaged every 3−4 days. For quantitative comparisons cells with identical passage numbers were used. The cells were counted with a hemocytometer.

Detection of Pgp Expression. The expression level of Pgp in wild-type (LLC-PK1 and NIH3T3) and transfected (LLC-MDR1, LLC-MDR1/V, and NIH-MDR-G185) cells was estimated using the monoclonal antibody MRK16, which recognizes only human Pgp. Aliquots of (2−3) × 10^5 cells were incubated in IMDM containing 5% FBS at 37 °C for 30 min in the presence of MRK16 or the unspecific antibody IgG_{2ak}. After washing, the cells were reincubated at 37 °C for 30 min in the dark, in the presence of the fluorescent FITC-labeled antibody. The cells were resuspended in phosphate-buffered saline (containing 1% BSA), and the fluorescence intensities for 10000 events per cell sample were analyzed using a FACSort flow cytometer (Becktron, Dickinson) and the software Win MDI for data analysis.

Cytosensor Measurement. ECARs of intact cells were measured using an eight-channel Cytosensor microphysiometer (Molecular Devices, Menlo Park, CA) described elsewhere in detail (*20*, *39*). The cells were seeded into 12 mm diameter polycarbonate cell capsule cups at a density of 3 × 10^5 cells per cup in culture medium. Usually the cells were incubated overnight at 37 °C before the measurement (*20*). This protocol was followed for measurements of relative ECARs (data shown in Figures 4, 7, and 8). For quantification of ECARs (data shown in Figures 2, 3, 5, 6, and 9) the cells were prepared 4 h prior to the Cytosensor experiment,

since the number of cells seeded remained approximately constant within this period of time. After incubation, capsule spacers and inserts were put into the cups, and the cells were thus located between two polycarbonate membranes which together with the spacer ring form a tight chamber of 2.8 μL with fluid contact to the potentiometric sensor chip. Measurements were performed at 37 °C. The acidification rates were measured during periodic interruptions of the flow of the medium through the flow chambers (for details see ref *20*). Each pump cycle lasted 2 min, during which time the pumps were on for 1 min 40 s and were then switched off for the remaining 20 s. During the pump-off period (from 1 min 45 s to 1 min 58 s) in each pump cycle the rate of extracellular pH changes were calculated by the Cytosoft program. The ECAR was determined as the slope of a linear least-squares fit to pH versus time data (μV/s), where −1 μV/s corresponds to an acidification rate of 0.001 pH unit/min at pH 7.4. After a constant acidification rate was reached (∼60−70 min), the flow medium was replaced by drug-containing medium. The cells were exposed to a 40 s pulse of a drug. The flow was then stopped, and the acidification rate was measured for 13 s. Perfusion with the drug solution was continued for another 2 min (the total drug perfusion interval was thus 160 s), and the ECAR was measured again (see ref *20*, Figure 1). The acidification rate was normalized to a basal acidification (defined as 100%) averaged over the two pump cycles before drug addition. The actual cellular response is given either in percentage over the basal activity or in absolute values of protons per cell, per second (H^+/cell/s).

Flow Medium and Buffer. The flow medium was prepared from the commercially available dry powder DMEM medium lacking sodium bicarbonate to have a low buffer capacity and to avoid formation of bubbles during the measurement. To preserve osmotic balance, sodium bicarbonate was replaced by sodium chloride (0.7 g of NaCl instead of 1 g of $NaHCO_3$). To adapt the cells to the conditions required for glucose deprivation and quantitative experiments, the flow medium was exchanged for flow buffer containing $CaCl_2$ (0.3 mM), $MgCl_2$ (0.6 mM), KH_2PO_4 (0.5 mM), KCl (3 mM), Na_2HPO_4 (0.5 mM), and NaCl (130 mM), with glucose (10 mM), $buffer_{g+}$, glucose and sodium pyruvate (1 mM), $buffer_{g+p+}$, no glucose but pyruvate, $buffer_{g-p+}$, or neither glucose nor pyruvate, $buffer_{g-p-}$. At the beginning of a measurement the pH of the solution was always adjusted to 7.4 at room temperature.

Quantification of Acid Export. To quantify the number of protons excreted by the cells within a certain time interval, the buffer capacity, β, and the number of cells in a flow chamber ($V = 2.8$ μL) have to be known. For flow buffer at pH 7.4 containing KH_2PO_4 (0.5 mM) and Na_2HPO_4 (0.5 mM) the buffer capacity was calculated according to Owicki (*24*) as $\beta = 0.40$ mM. For the phosphate salts we used a pK_a of 6.83 (6.865 at 25 °C) (*40*), which is in agreement with a value measured in our laboratory (X. Li Blatter, unpublished results) instead of the pK_a of 6.76 at 37 °C used previously (*20*, *24*). The buffer capacity of the DMEM flow medium is $\beta = 0.56$ mM, calculated as the sum of the buffer capacities of phosphate salts (0.91 mM) and amino acids, in particular glutamine (4 mM), histidine (0.2 mM), and cysteine (0.4 mM).

Due to the space limitation by the spacer, the number of cells in the measuring chamber, which give rise to the ECAR recorded by the sensor chip, corresponds to about 25% of the total cells seeded, that is $N_c = 0.75 \times 10^5$ cells, provided the cells are equally distributed in the capsule cup. Each of the sensors was calibrated at 37 °C with pH standard buffer solutions (Schott Glas, Mainz, Germany) within a range of pH of 6.81−8.87. According to the calibration, cal = 61.0 ± 1.1 mV corresponds to 1 pH unit. The ECARs (μV/s) recorded were transformed to protons released per cell per second as follows:

$$\text{ECAR } (H^+/\text{cell/s}) = [\text{ECAR (V/s)}][\beta\text{ (M)}][V\text{ (L)}]N_A/[\text{cal (V)}]N_c$$

where N_A is the Avogadro number. Units are given in parentheses.

Determination of Lactate Concentration. Total lactate production by NIH3T3 and NIH-MDR-G185 cells during basal and verapamil-induced metabolic rates was determined using a standard lactate spectrophotometric assay based on lactate oxidase and peroxidase activity (Sigma, Cat. No. 735-10, St. Louis, MO). The cells from 17−20 passages (9−10 weeks) were prepared as described before. The cells were perfused for ∼1 h in the Cytosensor with $buffer_{g+}$. Next, the cells were stimulated continuously for another 1 h with verapamil (6 μM) containing $buffer_{g+}$. The phosphate buffer leaving the Cytosensor chambers was collected, condensed by lyophilization, diluted 15 times with water, and assayed using the protocol provided by the lactic acid assay kit obtained from Sigma (which is adapted with minor changes from ref *41*). The number of lactate molecules produced per cell per second were calculated taking into account the total number of cells (3×10^5) placed on the capsule cup and an average flow rate of 83 μL/min, including pump-on and pump-off periods. In contrast to ECAR measurements where only about 25% of the cells are in contact with the sensor chip, all cells in the sensor chamber contribute to the acidification of the waste buffer leaving the sensor chamber.

Plasma Membrane Vesicle Preparation. The cell membranes were prepared as described previously (*42*) with some modifications. Briefly, cells washed once with PBS buffer were scraped into ice-cold PBS, pH 7.0, supplemented with protease inhibitors (1 tablet/50 mL of PBS). Next the cells were washed with hypotonic lysis buffer (10 mM Tris−HCl, pH 7.5, 10 mM NaCl, 1 mM $MgCl_2$, 1 protease inhibitor cocktail tablet/50 mL) by centrifugation at $2100g_{max}$ for 10 min at 4 °C. The pellet was resuspended in lysis buffer (5 mL per each of four 15 cm dishes) and was then frozen rapidly in dry ice. The frozen cell suspension was stored at −80 °C until later use. The cell suspension was thawed at room temperature and was then incubated on ice 30−45 min prior to the disruption of cells with a "One Shot" cell disrupter (Constant Systems Ltd., Warwickshire, U.K.) at 400 bar. The cell lysate was diluted 1:1 with ice cold isotonic buffer (10 mM Tris−HCl, pH 7.4, 250 mM sucrose, 50 mM *N*-methyl-D-glucamine, NMDG, 1 protease inhibitor cocktail tablet/50 mL buffer), and the unbroken cells and nuclei were precipitated by centrifugation at $800g_{max}$ for 10 min at 4 °C. Subsequently mitochondria were removed by centrifugation at $6000g_{max}$ for 10 min at 4 °C, and in the final centrifugation ($100000g_{max}$, 1 h, 4 °C) the crude membranes were pelleted.

The pellet was resuspended with isotonic buffer, homogenized by aspiration through a 23-gauge syringe, and stored at −80 °C until use. The protein content of the membrane vesicles (9−10 mg/mL) was determined by BCA protein assay using bovine serum albumin as a standard.

ATPase Activation Assay. The P-glycoprotein-associated ATPase activity in plasma membrane vesicles was measured as described previously (*42*) with an adjustment to the assay carried out in a 96-well microtiter plate, with a reaction volume of 40 μL/well. The membrane suspension (5−13 μg of protein) was first incubated for 5 min at 37 °C with ATPase assay buffer (50 mM Tris−HCl, pH 7.5, 150 mM NMDG, 5 mM sodium azide, 1 mM EGTA, 1 mM ouabain, 2 mM DTT, and 10 mM $MgCl_2$) with or without 0.3 mM sodium vanadate. The reaction mixture was then incubated for 3 min at 37 °C with 5 μL of verapamil stock solution (80 μM in water, containing 5% DMSO). The final verapamil concentration was 10 μM and the final DMSO concentration was 0.625% (v/v). The reaction was initiated by addition of ATP solution (final concentration 5 mM in 40 μL). After 20 min of incubation at 37 °C the reaction was stopped by addition of 30 μL of 10% (w/v) SDS. For the estimation of released inorganic phosphate (P_i) 250 μL of ice-cold medium (0.2% (w/v) ammonium molybdate, 1.3% (v/v) sulfuric acid, 2.3% (w/v) trichloroacetic acid, and freshly prepared 1% (w/v) ascorbic acid) was added to each well. After 100 min of incubation at room temperature the absorbance at 820 nm was measured using a Spectramax M2 microplate reader (Molecular Devices, Sunnyvale, CA). Control measurements were performed with the appropriate DMSO concentrations.

Error Calculations. The error bars given in Figures 2, 3, and 5−9 correspond to standard deviations, SDs. The statistical significance of the data in Figure 6 was calculated with the Student's *t* test.

RESULTS

Expression Level of Pgp in MDR1-Transfected Cell Lines. The level of Pgp expression in *MDR1*-transfected cells (LLC-MDR1, LLC-MDR1/V, and NIH-MDR-G185) and the corresponding wild-type cells (LLC-PK1 and NIH3T3) was studied by FACS using the monoclonal antibody MRK16 and a fluorescent, FITC-labeled second antibody. Figure 1 displays the cell count as a function of the relative fluorescence intensities (logarithmic scale) for the different cell lines studied. Cells overexpressing human Pgp (lines 1, 2, and 4) exhibit distinctly higher fluorescence intensity than wild-type cells (lines 3 and 5). Whereas LLC-MDR1/V cells grown in the presence of vincristine (line 1) and NIH-MDR-G185 grown in the presence of colchicine (line 4) show one population at high fluorescence intensity, LLC-MDR1 cells grown in the absence of vincristine show two populations, the first one at low (∼25% of the cells) and the second one at high fluorescence (∼75% of the cells) intensity. The content of human Pgp in the whole cell population was expressed as the ratio of the median fluorescence intensities (MFIs) of MRK16-labeled cells and isotype control IgG2a-labeled cells. It increases in the order wild-type cells (MFI = 1) < LLC-MDR1 (MFI = 23) < LLC-MDR1/V (MFI = 38) < NIH-MDR-G185 (MFI = 79). The expression level of endogenous Pgp in wild-type (2ac.1, 2ac.2, NIH3T3 (*38*), LLC-PK1 (*43*)), *Mdr1a*$^{-/-}$*1b*$^{-/-}$ knockout (*38*), and LLC-MRP1 (*37*) cells has been estimated previously by means of Western blot analysis and was not further analyzed. The expression level of Pgp thus increases in the order *Mdr1a*$^{-/-}$*1b*$^{-/-}$ knockout cells (77.1, 88.6) < wild-type cells (2ac.1, 2ac.2, LLC-PK1, NIH3T3) ≈ LLC-MRP1 < LLC-MDR1 < LLC-MDR1/V < NIH-MDR-G185. Experiments were performed with cells of higher passage number (pn > 4). In the following we assume that the expression level of Pgp does not change with the passage number in the range of 2−20 passages after defreezing.

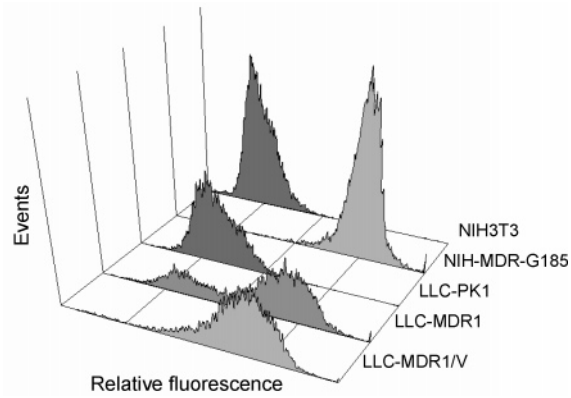

FIGURE 1: Expression of human Pgp monitored by immunoflow cytometry, FACS. Histograms represent the cell number versus fluorescence intensity expressed as the logarithm of the relative fluorescence intensity. Each distribution was obtained from collecting 10^4 cells labeled with MRK16 antibody. Transfected cell lines LLC-MDR1/V (grown in the presence of vincristine (0.32 μM)) (line 1), LLC-MDR1 (line 2), and NIH-MDR-G185 (grown in the presence of colchicine (0.15 μM)) (line 4) are shown in light gray and the corresponding wild-type cells LLC-PK1 (line 3) and NIH3T3 (line 5) in dark gray. Cells of high passage numbers (pn > 4) were used.

Basal ECARs of the Different Genetically Modified Cell Lines. ECARs were monitored by means of a Cytosensor microphysiometer with four or eight parallel measuring chambers. Each chamber contained a potentiometric sensor chip measuring the extracellular acidification rate (μV/s) during periodic interruptions of the flow of the medium through the flow chambers (*19*). At 61 mV/pH unit and taking into account the buffer capacity, β, of the flow medium, the net flow of protons per second per cell was calculated (cf. Materials and Methods).

In our previous investigations MEM or DMEM was used as the flow medium to measure Pgp activation (*20*). However, since the effect of nutrients on the Pgp-induced cell activity was to be studied, the present measurements were made with simple buffer solutions. We first compared the basal ECARs of the different cell lines in DMEM with those obtained with phosphate buffer containing 10 mM glucose ($buffer_{g+}$) to test whether cellular metabolism was affected by the omission of the amino acids and vitamins present in DMEM. For this purpose, the cells were first exposed to DMEM (buffer capacity β = 0.56 mM) until stable basal ECARs were reached (75 min). DMEM was then replaced by glucose-containing $buffer_{g+}$ (buffer capacity β = 0.40 mM). Parts A (DMEM) and B ($buffer_{g+}$) of Figure 2 display the ECARs of the 10 cell lines employed in this study, ordered according to increasing expression levels of Pgp, that is, *Mdr1a*$^{-/-}$*1b*$^{-/-}$ knockout cells (77.1, 88.6) < wild-type cells (2ac.1, 2ac.2, LLC-PK1, NIH3T3) ≈ LLC-MRP1 < LLC-MDR1 < LLC-MDR1/V < NIH-MDR-

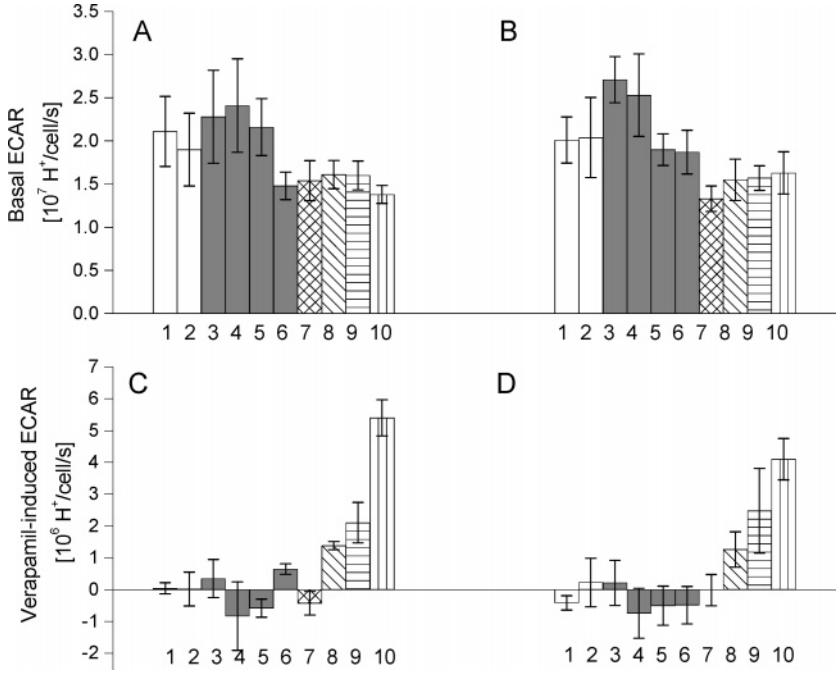

FIGURE 2: Basal extracellular acidification rates, ECARs (A, B), and verapamil (10 μM)-induced ECARs after subtraction of the basal ECARs (C, D) of *Mdr1a*$^{-/-}$*1b*$^{-/-}$ knockout cells 77.1 (1) and 88.6 (2) (white columns), wild-type cells 2ac.1 (3) 2ac.2 (4), LLC-PK1 (5), and NIH3T3 (6) (gray columns), and cells transfected with *MRP1* or *MDR1* genes, LLC-MRP1 (7), LLC-MDR1 (8), LLC-MDR1/V (9), and NIH-MDR-G185 (10) (patterned columns). The cells were exposed to DMEM (A, C) or to phosphate buffer containing 10 mM glucose (B, D). The cells were defrozen 2−3 passages prior to the measurements. Error bars correspond to $n = 3-4$ measurements.

G185. After correction for the different buffer capacities, the ECARs of a given cell line in DMEM and in glucose buffer$_{g+}$ were practically identical. Furthermore, parts A and B of Figure 2 demonstrate that the basal ECARs of the different cell lines are similar and in the range of (1.4 ± 0.1) × 10^7 to (2.4 ± 0.5) × 10^7 H^+/cell/s (−66 ± 5 to −117 ± 26 μV/s) for DMEM and (1.3 ± 0.2) × 10^7 to (2.7 ± 0.3) × 10^7 H^+/cell/s (−89 ± 10 to −183 ± 18 μV/s) for buffer$_{g+}$. However, the ECARs of wild-type cells (gray columns) are on average 30 ± 10% larger than those of knockout (white columns) and transfected (patterned columns) cells. Considering only *MDR1*-transfected and the corresponding wild-type cells, the difference is lower (20 ± 4%). For the experiments shown in Figure 2 cells from a narrow range of cell passages after defreezing (pn = 2−3) were used to get optimal synchronization of cells.

The number of cell passages had a distinct influence on the ECAR as exemplified in Figure 3 for NIH-MDR-G185 cells, knockout cells (77.1), and the corresponding wild-type cells. At low passage numbers (pn = 2−3) the ECARs were lower than at higher passage numbers (pn ≥ 4). Basal ECARs of the second data set with high passage numbers, analogous to those in Figure 2, were on average over all cell lines 60 ± 40% higher than those of low passage numbers, whereby the difference between the basal ECARs of low and high passage numbers was lower (∼20%) for *Mdr1a*$^{-/-}$*1b*$^{-/-}$ knockout cells (77.1, 88.6) and the corresponding wild-type cells (2ac.1, 2ac.2) and higher (80−100%) for transfected cells (LLC-MRP1, LLC-MDR1, LLC-MDR1/V, NIH-MDR-G185). At higher passage numbers (pn > 4) the difference in ECARs between NIH-MDR-G185 and the corresponding wild-type cells therefore practically disappeared (Figure 5A).

Basal ECARs under Starvation Conditions. Next the activity of NIH-MDR-G185-transfected cells was tested after withdrawal of exogenous carbon sources. The metabolic response is seen in Figure 4. During period A, cells were perfused with buffer$_{g+}$ until a stable basal ECAR was reached. A preequilibration period of ∼60 min is not shown. The basal ECAR was normalized and defined as 100%. As a control, perfusion with glucose buffer (buffer$_{g+}$) was continued in one chamber (■, no change in the ECAR occurring).

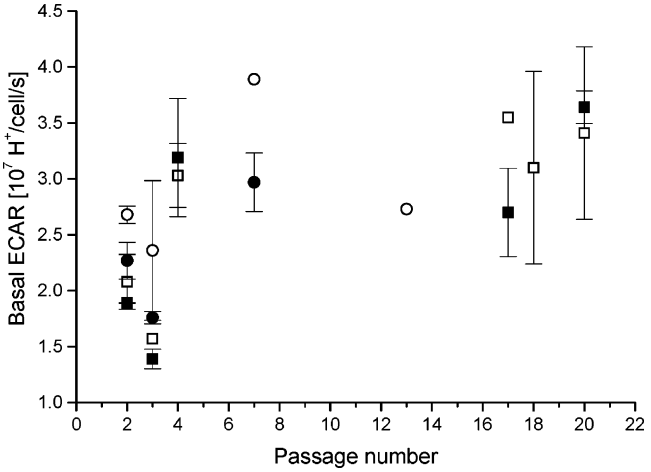

FIGURE 3: Basal extracellular acidification rate as a function of the passage number of NIH-MDR-G185 (■), NIH3T3 (□), *Mdr1a*$^{-/-}$*1b*$^{-/-}$ knockout cells 77.1 (●) and 2ac.2 (○) cells as a function of the passage number. Measurements were performed in phosphate buffer containing 10 mM glucose. Error bars correspond to $n = 2-6$ measurements.

When sodium pyruvate (1 mM) was added to glucose buffer (buffer$_{g+p+}$, ▼), a significant decrease in the ECAR was observed. Pyruvate (1 mM) without glucose (buffer$_{g-p+}$, ○) led to an even larger decrease in the ECAR. Complete

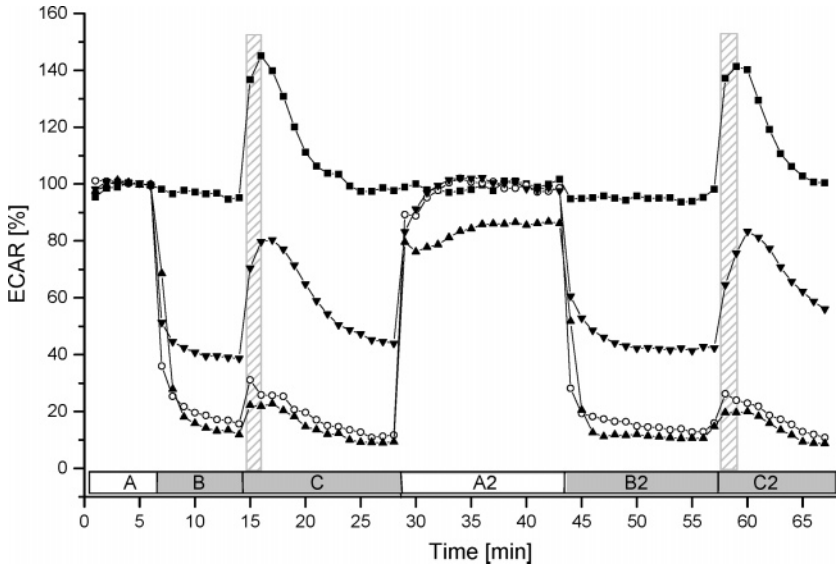

FIGURE 4: Effect of glucose and sodium pyruvate on the basal and verapamil-induced acidification rate of NIH-MDR-G185 cells. Cells of high passage numbers were used (pn > 20). During period A (indicated in white), the cells in all four chambers were exposed to phosphate buffer with glucose, buffer$_{g+}$. During periods B and C (indicated in gray) only one chamber was perfused with buffer$_{g+}$ (■); the others were perfused with buffer containing in addition 1 mM sodium pyruvate, buffer$_{g+p+}$ (▼), buffer containing 1 mM sodium pyruvate without glucose, buffer$_{g-p+}$ (○), or buffer containing neither glucose nor pyruvate, buffer$_{g-p-}$ (▲). Periods A−C were repeated (A2, B2, C2). Hatched bars indicate the interval (160 s) during which the cells were perfused with verapamil (6 μM). The basal ECAR of cells in buffer$_{g+}$ was defined as 100%. Results are normalized to the baseline and are expressed as a percent of the basal acidification rate.

elimination of all carbon sources (buffer$_{g-p-}$, ▲) caused a further small decrease.

Comparing the different cell lines, the average reduction of basal ECARs due to addition of pyruvate was more pronounced for mouse embryo fibroblasts (50 ± 10%, wild-type and transfected NIH cells) than for pig kidney cells (15 ± 4%, wild-type and transfected cells) (not shown). If glucose was removed or replaced by its nonmetabolizable analogue deoxyglucose, the basal ECARs of all cell lines tested were reduced by 75−90%.

Figure 5A then compares the basal ECARs of wild-type and transfected cells in the presence (□, ■) and absence (○, ●) of glucose, where open and closed symbols represent ECARs of cells with low (pn = 2−3) and high (pn = 4−20) passage numbers, respectively. Basal ECARs (logarithmic scale) are plotted as a function of the median fluorescence intensity representing the expression level of human Pgp. As a general conclusion it follows that under equivalent conditions of nutritional state and passage number wild-type and *MDR1*-transfected cells exhibit rather similar metabolic activity.

Verapamil-Induced Extracellular Acidification Rates. Figure 4, period C, displays the variation of the ECARs of NIH-MDR-G185 cells upon addition of verapamil under different nutritional conditions. We first discuss verapamil effects under normal nutritional conditions, that is, when the cells are perfused with buffer$_{g+}$ (uppermost curve in Figure 4, ■). At the beginning of period C, verapamil was added to buffer$_{g+}$ at a concentration of 6 μM during 160 s (hatched bar). After this stimulation interval the cells were again perfused with buffer$_{g+}$. Immediately after stimulation, the ECAR increases, indicating a distinct increase in acid production induced by verapamil. After the return to normal buffer$_{g+}$ the ECAR returns to basal values. Analogous measurements were performed for all 10 cell lines, and the quantitative evaluation for cells with pn = 2−3 is summarized in Figure 2C,D. The values given correspond to the ECAR increase measured at the end of the 160 s stimulation interval. The verapamil-induced ECARs in DMEM (Figure 2C) and buffer$_{g+}$ (Figure 2D) are practically identical. Parts C and D of Figure 2 show that an increase in ECARs upon verapamil stimulation is observed only for cells overexpressing P-glycoprotein (columns 8−10), and that the increase in ECARs is proportional to the expression level of Pgp (see also Figure 5B,C).

We then tested whether Pgp activation by verapamil was still possible under starvation conditions. As seen in Figure 4, period C, verapamil stimulation induced a distinct ECAR increase under all buffer conditions, even in the absence of exogenous carbon sources. The stimulation cycle in Figure 4 (periods A−C) was then repeated. In period A2 the cells were again perfused with buffer$_{g+}$ in all four chambers. Cells treated with buffer$_{g+p+}$ (▼) and buffer$_{g-p+}$ (○) during periods B and C reversed to the initial ECARs within 5 min, whereas cells treated with buffer$_{g-p-}$ (▲) did not recover completely even after 15 min. Verapamil stimulation in period B2 yielded results very similar to those of period B. Even cells in buffer$_{g-p-}$ which had not recovered completely showed a similar ECAR upon the second verapamil stimulation.

The verapamil stimulation cycle in Figure 4 was repeated for a third time (data not shown) to test inhibition of verapamil-induced ECARs by cyclosporin A. For this purpose, cyclosporin A (1 μM) was added to the four different buffers and NIH-MDR-G185 cells were preincubated for 20 min followed by stimulation with verapamil, again in the presence of cyclosporin A. This led to an inhibition of the verapamil-induced ECARs by 50−60% under all buffer conditions, in agreement with previous inhibition values (*20*).

Parts B and C of Figure 5 display the *absolute* and *relative* increase in ECARs upon verapamil stimulation (10 μM) of *MDR1*-transfected and wild-type cells in the presence (□,

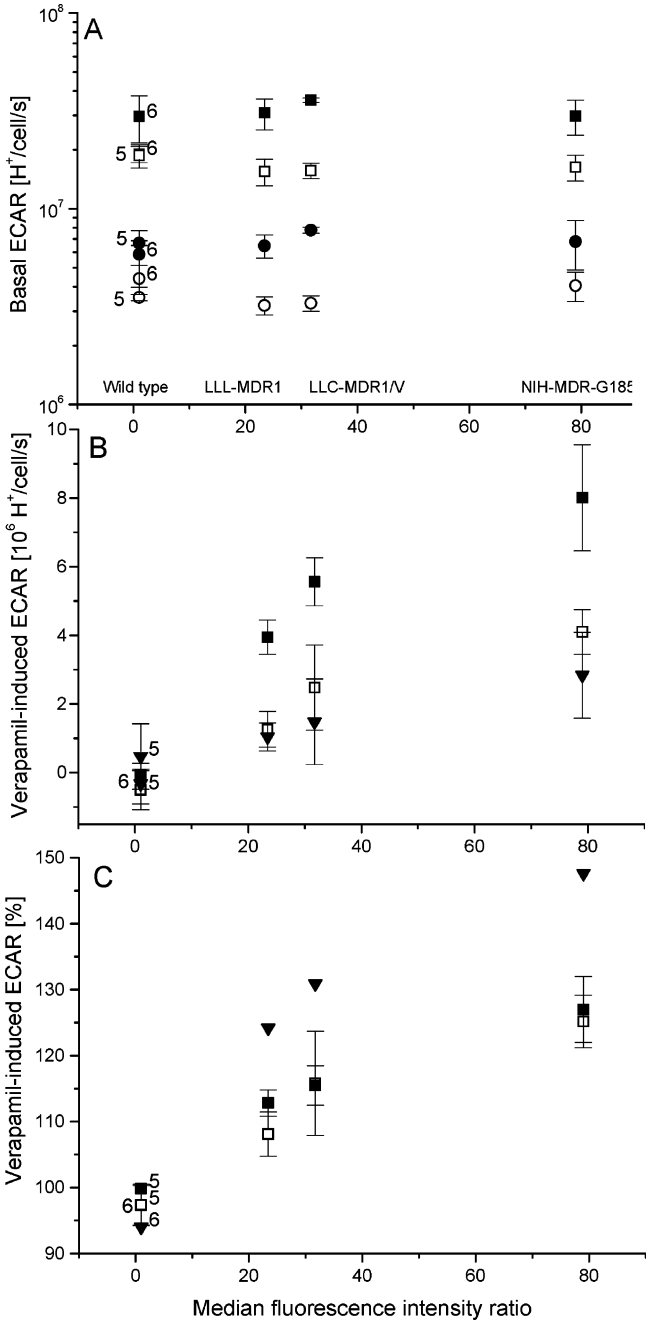

FIGURE 5: Basal (A) and verapamil (10 μM)-induced ECAR as a function of the expression level of human Pgp in cells given in absolute values (B) and relative values, where basal ECARs were taken as 100% (C). The expression level of Pgp was determined by FACS analysis and is expressed in MFIs for wild-type cells (MFI = 1) (LLC-PK1 (label 5), NIH3T3 (label 6)) and *MDR1*-transfected cells (LLC-MDR1 (MFI = 23), LLC-MDR1/V (MFI = 38), NIH-MDR-G185 (MFI = 79)). The cells for ECAR experiments were defrozen either 2−3 passages or 4−20 passages prior to the measurements, and the values given correspond to an average of $n = 3-4$ (□, ○) or $n = 2-17$ (■, ●) measurements. Both sets of data were measured in the presence ($buffer_{g+}$) (squares) and absence ($buffer_{g-p-}$) (circles) of glucose. Verapamil-induced ECARs (B, C) in the absence of glucose are shown as average values of all measurements ($n = 4-21$) for cells defrozen 2−20 passages prior to the measurements (▼).

■) and absence (▼) of glucose plotted as a function of the expression level of Pgp. Under all conditions ECARs increased with the expression level of Pgp. *Absolute* ECARs (Figure 5B) were higher in the presence (□, ■) than in the absence (▼) of glucose. However, if expressed as percent changes *relative* to the corresponding basal ECAR (Figure 5C), glucose-deprived cells showed a distinctly larger verapamil-induced stimulation than glucose-fed cells.

ECARs of cells with higher passage numbers (pn = 4−20) (■) are higher than those of cells from low passage numbers (pn = 2−3) (□) if given in absolute values (Figure 5B). However, if again expressed as percent changes of basal ECARs, the two data sets are practically identical (Figure 5C). For the sake of clarity, the data obtained for glucose-deprived cells with low and high passage numbers were averaged in Figure 5B,C (▼). The largest relative increase is clearly observed for cells under starvation conditions (cf. also Table 1).

Rate of Lactic Acid Efflux. NIH-MDR-G185 and NIH3T3 cells were perfused with glucose-containing $buffer_{g+}$ in the Cytosensor. The buffer was collected after leaving the chamber and was tested for lactate using a spectrophotometric assay based on lactate oxidase and peroxidase activity. Figure 6 shows the rate of lactate molecules exported (hatched columns) by NIH3T3 and NIH-MDR-G185 cells under basal conditions (−) and when stimulated continuously with 6 μM verapamil (+) for ∼1 h. The lactate rates are compared to the proton efflux rates (ECARs) measured in parallel (gray columns).

In the absence of verapamil, NIH3T3 and NIH-MDR-G185 cells exported $(3.5 \pm 0.5) \times 10^7$ and $(3.0 \pm 0.9) \times 10^7$ lactates/cell/s, respectively. The basal ECARs determined in parallel corresponded to $(3.4 \pm 0.1) \times 10^7$ and $(3.0 \pm 0.6) \times 10^7$ H^+/cell/s for NIH3T3 cells and NIH-MDR-G185 cells, respectively (see also Table 1).

Verapamil (6 μM) induced an increase in the rate of lactate export and in the ECAR of $(4.8 \pm 1.5) \times 10^7$ lactates/cell/s and $(4.5 \pm 0.4) \times 10^7$ H^+/cell/s, respectively, in Pgp-overexpressing cells. In wild-type cells, the rate of lactate export and the ECAR remained at $(3.4 \pm 0.5) \times 10^7$ lactates/cell/s and $(3.3 \pm 0.5) \times 10^7$ H^+/cell/s. Data in Figure 6 thus demonstrate that the rate of lactic acid leaving the measuring chambers of the Cytosensor corresponds to the rate of extracellular acidification registered by the pH-sensitive potentiometric sensor chip in the measuring chamber of the Cytosensor.

Route of Lactic Acid Efflux. To identify the pathway of lactic acid efflux, we incubated the cells in the Cytosensor chambers with DIDS and phloretin, which inhibit inorganic anion exchange mechanisms and monocarboxylate carriers, respectively (*44*, *45*). Figure 7 shows the influence of DIDS and phloretin on basal ECARs of NIH-MDR-G185, LLC-MDR1, and NIH3T3 cells. Exposure of cells to increasing concentrations of DIDS (50−600 μM) leads to a slow decrease in basal ECARs. After 20 min of incubation with DIDS a reduction by about 10−15% was reached in wild-type and transfected cell lines. In contrast, exposure of NIH-MDR-G185 and NIH3T3 cells to phloretin leads to a fast decrease by ∼60% and ∼70%, respectively, which remained constant after 6 min.

Figure 8 shows the effect of DIDS and phloretin on verapamil-induced ECARs in NIH-MDR-G185 and NIH3T3 cells. The cells were preincubated with DIDS or phloretin for 20 and 6 min, respectively, and were then stimulated with 6 μM verapamil for 160 s in the presence of DIDS or phloretin. DIDS had no effect on the ECAR in the whole

Table 1: Basal and Verapamil-Induced Rate of Proton and Lactate Export by NIH-MDR-G185 and NIH3T3 Cells in $Buffer_{g+}$ under Different Conditions

no. of cell passages after defreezing	verapamil (μM)	10 mM glucose	stimulation time	basal ECAR for NIH3T3 [10^7 H^+/cell/s]	basal ECAR for NIH-MDR-G185 [10^7 H^+/cell/s]	verapamil-induced ECAR for NIH-MDR-G185 [10^6 H^+/cell/s]	verapamil-induced relative to basal (100%) ECAR for NIH-MDR-G185 (%)
2−3	10	+	160 s	1.87 ± 0.25 (3)[a]	1.63 ± 0.24 (4)[a]	4.1 ± 0.6 (4)[a]	125
4−20	10	+	160 s	2.97 ± 0.80 (10)	2.98 ± 0.60 (17)	8.0 ± 1.5 (16)	127
2−20[b]	10	−	160 s	0.54 ± 0.17 (13)	0.60 ± 0.21 (21)	2.8 ± 1.2 (20)	148
17−20	6[c]	+	60 min	3.40 ± 0.14 (3)	3.05 ± 0.58 (9)	14.7 ± 4.2 (9)	148
17−20	6	+	60 min	3.48 ± 0.45[d] (3)	3.03 ± 0.91[d] (9)	17.4 ± 15[d] (9)	157[d]

[a] Numbers in parentheses correspond to the numbers of measurements. [b] Since ECARs are relatively weak for glucoses-deprived cells, an average value of low (2−3) and high (>4) passage numbers is given. [c] ECAR measurements as a function of verapamil concentration have shown that ECAR values for 6 and 10 μM verapamil are very similar (*20*). [d] Amount of lactate determined spectrophotometrically (lactates/cell/s).

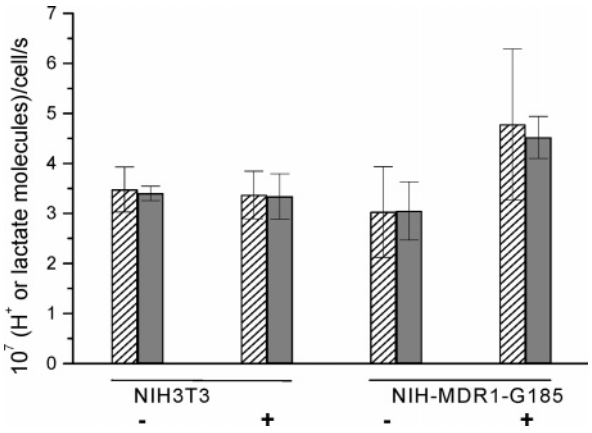

FIGURE 6: Comparison between the rate of lactic acid efflux as determined spectrophotometrically (hatched columns) and the extracellular acidification rate as determined by means of the Cytosensor microphysiometer (gray columns) for NIH3T3 ($n = 3$) and NIH-MDR-G185 ($n = 9$) cells in the absence (−) and presence (+) of 6 μM verapamil. The cells were defrozen 17−20 passages prior to the measurements. The differences in lactate efflux (and ECAR) between NIH-MDR-G185 without and with verapamil are statistically significant ($p < 0.05$) (and $p < 0.001$).

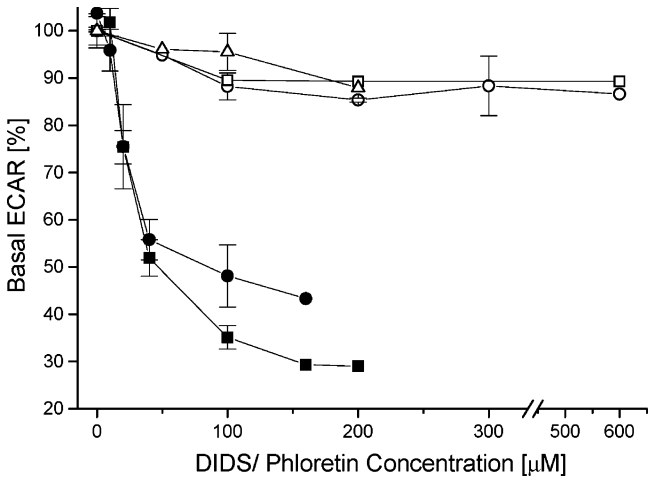

FIGURE 7: Effect of increasing concentrations of DIDS (open symbols) and phloretin (solid symbols) on the basal ECARs of NIH-MDR-G185 (circles), NIH3T3 (squares), and LLC-MDR1 (triangles) cells. The basal ECAR was defined as 100%. Results are normalized to the baseline and are expressed as a percent of the basal rate.

concentration range investigated (50−300 μM) (Figure 8A), suggesting that inorganic ion exchange mechanisms play no significant role in lactate efflux in intact cells. On the other hand, phloretin completely inhibited the Pgp-specific ECAR

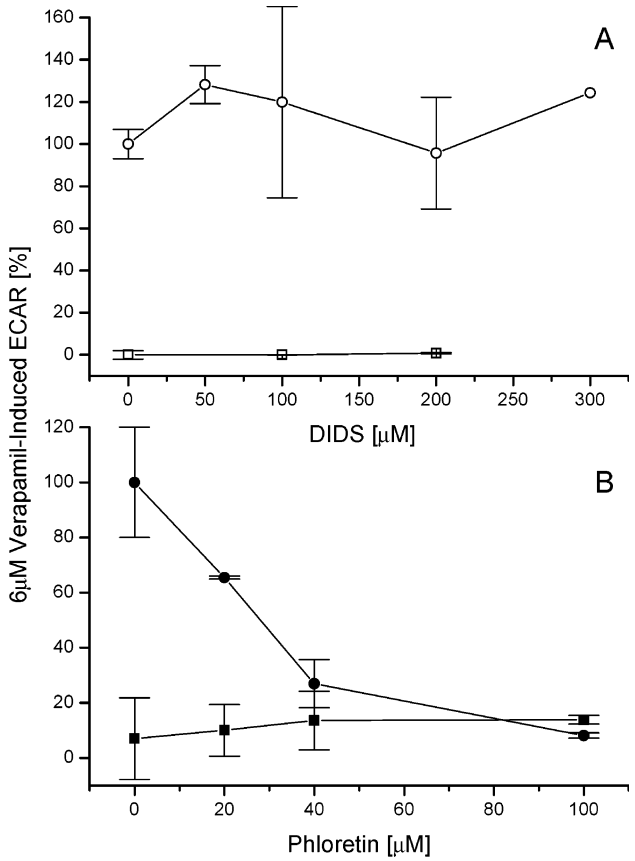

FIGURE 8: Effect of increasing concentrations of DIDS (A, open symbols) and phloretin (B, solid symbols) on verapamil (6 μM)-induced ECARs of NIH-MDR-G185 (circles) and NIH3T3 (squares). The ECARs of cells stimulated with verapamil for 160 s minus the corresponding basal ECARs (in the absence of inhibitors) were defined as 100%. Results are normalized and expressed as a percent of the verapamil-induced ECAR subtracted from the basal ECAR.

at a concentration of 100 μM, suggesting that monocarboxylate carriers are involved in lactate export (Figure 8B). As will be discussed below phloretin may, however, also affect glucose import. The concentration of 50% inhibition of lactate export by phloretin was $IC_{50} = 47 \pm 20$ μM (40 ± 19 μM) for wild-type (transfected) cells under basal conditions and $IC_{50} = 22 \pm 8$ μM for transfected cells upon drug activation.

ATPase Activation Assay. Basal Pgp activation led to a phosphate release of 10.7 ± 0.9 (nmol/mg of total protein)/min. Activation of the Pgp ATPase in plasma membrane vesicles of NIH-MDR1-G185 cells at pH 7.5 by verapamil

(10 μM) led to an increase in phosphate release by 14.1 ± 2.3 (nmol/mg of total protein)/min.

Taking into account the number of cells, the molecular mass of Pgp (170 kDa), and the total protein concentration determined experimentally, the content of Pgp was calculated as 0.85 ± 0.23% of total protein, in good agreement with previous results (*46*, *47*). By combining these results with the estimate of the number of Pgp molecules per cell in NIH-MDR1-G185 (*8*), we calculated the turnover number of verapamil-induced activity as 4.7 ± 0.8 ATP hydrolyzed/Pgp/s. The errors correspond to four measurements.

DISCUSSION

Up to now, the classical method to determine Pgp-ATPase activation was based on inorganic phosphate release measurements made with inside-out vesicles prepared from Pgp-overexpressing cells. This method has the disadvantage that it is rather time-consuming and also requires destruction of the living cell. Therefore, little is known on the role of the basal metabolic state of the cell for Pgp activation. We have recently shown (*20*) that measuring the extracellular acidification rate of living *MDR1*-transfected cells by means of a Cytosensor (*19*) provides a much faster and more convenient method to monitor Pgp-ATPase activation. In the present study we have developed this method further. Our main interest is to investigate the influence of the metabolic state of the cell, which depends on the cell culture time (passage numbers) as well as on the nutritional state of the cell. We considered drug-induced stimulation of Pgp under conditions of starvation in some detail to understand the mechanism of extracellular acidification in relation to the general glycolytic metabolism of the cell and to show how it is linked to Pgp-induced ATP hydrolysis under conditions of Pgp activation.

The Different Genetically Modified Cell Lines Show Similar ECARs. For a comparison of the different cell lines the cells were kept in culture for identical periods of time after defreezing. Basal ECARs of wild-type (2ac.1, 2ac.2, LLC-PK1, NIH3T3) and genetically modified (*Mdr1a*$^{-/-}$*1b*$^{-/-}$ knockout, *MDR1*- and *MRP1*-transfected (LLC-MDR1, LLC-MDR1/V, NIH-MDR-G185, LLC-MRP1)) cell lines were on the order of 10^7 H^+/cell/s, whereby those of genetically modified cells were on average slightly lower than those of wild-type cells (Figure 2 and 5, Table 1). The expression level of Pgp as such had no influence on the basal extracellular acidification rate of the different cell lines (Figures 2 and 5).

Basal Metabolic Rates Depend on Cell Culture Time. The rate of cellular metabolism reflected by the ECAR depends on many factors such as temperature, pH, ionic strength, and nutritional conditions (glucose concentration). The present data demonstrate that it also depends on the time which cells spend in culture after defreezing. For the comparison of different cell lines we collected two data sets, one for cells of low passage numbers (pn = 2−3) and one for cells of higher passage numbers (pn = 4−20), where the former show lower acidification rates than the latter (Figure 3, Table 1). A stable situation was reached after about two weeks in culture (pn ≥ 4). Basal ECARs in buffer$_{g+}$ as well as in medium (DMEM) were in the range of 1.3×10^7 to 2.7×10^7 H^+/cell/s for cells of low passage numbers (pn = 2−3).

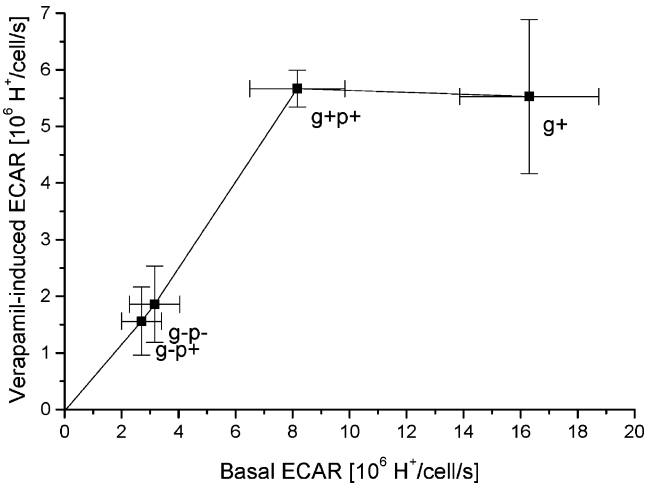

FIGURE 9: Contribution of exogenous carbon sources to the basal and verapamil-induced ECARs of NIH-MDR-G185 cells. The cells were perfused with phosphate buffer without any carbon sources (buffer$_{g-p-}$), with 1 mM pyruvate (buffer$_{g-p+}$), 1 mM pyruvate and 10 mM glucose (buffer$_{g+p+}$,), or 10 mM glucose (buffer$_{g+}$). Data in buffer$_{g-p+}$ correspond to an average of the data shown in Figure 4, data in buffer$_{g+}$ correspond to an average of the data from Figures 2B,D and 4, and data in buffer$_{g+p+}$ and buffer$_{g-p-}$ correspond to an average of the data from Figure 4 and two additional sets of measurements (n = 3−4), not shown. The line is drawn to guide the eyes.

The basal metabolism reflected by the ECAR is thus generally more affected by variations in the cell culture time (60 ± 40%, depending on the cell line) than by transfection (30 ± 10% for pn = 2−3, depending on the cell line).

ECARs due to Verapamil Stimulation Increase with the Expression Level of Pgp and Depend on the Metabolic State of the Cell. A metabolic response to verapamil stimulation was observed for *MDR1*-transfected cells only (Figures 2C,D and 5) and increased with the expression level of Pgp. In absolute terms, the response to verapamil stimulation was higher for cells of high passage numbers (pn = 4−20) than of low passage numbers (pn = 2−3). However, verapamil-induced ECARs relative to basal values were practically identical for the two data sets (cf. Figure 5C). This suggests that Pgp activation and the concomitant protection of cells against drugs and toxins are directly proportional to the basal metabolic state of the cell.

The metabolic conditions of the cells were modified by perfusing the cells in the Cytosensor either with buffers containing pyruvate in the presence or absence of glucose or with a buffer lacking a carbon source. To illustrate the amount of energy spent by NIH-MDR-G185 cells on detoxification by Pgp relative to the basal metabolic energy under different nutritional conditions, basal ECARs were plotted versus the verapamil-induced ECARs (Figure 9).

Addition of pyruvate (1 mM) to glucose-containing buffer (buffer$_{g+p+}$) led to a 50% decrease of the basal ECAR. Despite the decrease in basal metabolism, the verapamil-induced ECAR remained as high as in buffer$_{g+}$. The energy required to activate Pgp in the presence of pyruvate (buffer$_{g+p+}$) thus required on average ∼50% of the basal ECAR in contrast to only ∼25% in buffer$_{g+}$.

If pyruvate was the only carbon source (buffer$_{g-p+}$) or if exogenous carbon sources were lacking (buffer$_{g-p-}$), the absolute ECAR or the rate of basal metabolism decreased further (cf. Table 1). Nevertheless, Pgp activation by

verapamil was still possible and comprised again 50−60% of the basal value.

An analogous behavior was observed for LLC-MDR1 and LLC-MDR1/V cells. While the ECARs of LLC-MDR1 and LLC-MDR1/V cells upon verapamil stimulation (10 μM) were 108 ± 3% and 116 ± 7%, respectively, in the presence of glucose, they amounted to 124% and 131%, respectively, in the absence of exogenous carbon sources.

The reduction of the basal ECAR in the presence of high pyruvate concentrations led to substrate inhibition of lactate dehydrogenase (*48*). However, when Pgp was stimulated by verapamil and the ATP requirement was enhanced, glycolysis was up-regulated even in the absence of exogenous carbon sources. This suggests that endogenous carbon sources are used to drive Pgp under conditions of starvation.

Somewhat higher ECARs were also observed upon long-time (60 min) exposure to drugs (cf. Table 1). The value measured is in good agreement with previous results obtained in cancer cells under comparable conditions (*22*).

Glycolytic Pathway for Energy Production. For all cell lines basal ECARs were strongly reduced in the presence of pyruvate or deoxyglucose and in the absence of glucose as shown in Figure 4 for NIH-MDR-G185 cells, which is consistent with a primarily glycolytic pathway for energy production. Related results were obtained previously with Chinese hamster ovary cells CHO-K1 (*19*), swim bladder gas gland cells (*49*), and human rhabdomyosarcoma TE671 cells (*50*).

An analysis of the flow buffer leaving the Cytosensor measuring chambers containing NIH-MDR-G185 or NIH3T3 cells perfused with glucose-containing $buffer_{g+}$ revealed that the rate of lactate export was identical to the rate of proton export as determined by the potentiometric sensor chip (Figure 6), which further supports the primarily glycolytic pathway of these cells. We thus conclude that one molecule of lactate is exported per molecule of ATP synthesized.

To maintain cellular homeostasis, lactic acid molecules produced upon ATP synthesis must be transported across the cell membrane to the extracellular space. Multiple mechanisms exist, including facilitated transport by monocarboxylate carriers and anion exchange proteins as well as diffusion of the protonated acid across the membrane (*24*). Whether facilitated lactate export occurs by inorganic anion exchange mechanisms or by monocarboxylate carriers was tested by treating the cells with increasing concentrations of DIDS or phloretin, respectively. While DIDS reduced basal ECARs only by about ~10%, in agreement with previous measurements (*51*), phloretin reduced basal ECARs by about 70% in wild-type cells, and by about 60% in *MDR1*-transfected cells. The concentration of 50% inhibition of lactate export by phloretin was determined, in good agreement with previous measurements for other cell lines (IC_{50} = 3−40 μM) (*45*, *52*, *53*), suggesting that monocarboxylate transporters play an important role in lactate−proton cotransport. However, phloretin also inhibits the glucose transporter with a similar concentration of half-maximum activation (IC_{50} = 0.24−48 μM) (*49*, *54*, *55*). On the basis of the present experiments, it is therefore not possible to unambiguously decide to what extent inhibition of lactate export by phloretin is due to the inhibition of monocarboxylate transporters and to what extent it is due to the inhibition of glucose import and the concomitant reduction in basal metabolism.

The amount of lactic acid leaving the cell by passive diffusion is determined by the pK_a value of lactic acid (pK_a = 3.8) and the pH close to the cytosolic membrane surface (pH ≈ 5.5). At pH ≈ 7.0 lactate is fully dissociated, which prevents passive diffusion. However, close to the inner cytosolic membrane surface, which exhibits a negative surface potential, the concentration of protons is higher and the pH is therefore lower. As a consequence about 1% of the lactate molecules produced are protonated in this environment and can leave the cell by passive diffusion.

Proton−Drug Symport? On the basis of the fact that the large majority of drugs transported by Pgp are cationic (pK_a ≈ 8) and that Pgp can transport permanently charged cations (*56*), we have previously (*20*) discussed the possibility that proton efflux in *MDR1*-transfected cells could also arise from the transport of protonated drugs (proton−drug symport). A drug molecule inserted into the negatively charged cytosolic membrane interface, which is assumed to be the site of interaction between Pgp and its substrates, is likely to be protonated due to the slightly acidic environment close to the membrane surface and might thus get transported in its charged form. Since the extracellular aqueous phase is slightly acidified by lactic acid efflux, the proton would not dissociate from the drug molecule and would therefore most likely remain undetected by the Cytosensor. For truncated LmrA, a bacterial transporter related to Pgp, a proton−ethidium symport was indeed demonstrated recently, and was also proposed for the native transporter (*57*).

ATP Synthesis and ATP Hydrolysis. We have demonstrated that drug-stimulated ECARs correspond to the rates of lactic acid export, which suggests that the ECARs reflect in turn the rates of ATP synthesis. To investigate the relationship between the rate of ATP synthesis and the rate of ATP hydrolysis in more detail, we compared the number of lactic acid molecules exported (or the number of ATP molecules synthesized) per NIH-MDR1-G185 cell with the number of phosphate molecules released upon ATP hydrolysis in inside-out vesicles of the same cells upon stimulation with 10 μM verapamil. To estimate the number of phosphate molecules, P_i, released per cell, we multiplied the turnover number, which gives the number of molecules of ATP hydrolyzed (or the number of inorganic phosphate molecules released) per molecule of Pgp, determined as 4.7 ± 0.8 P_i/Pgp/s in inside-out vesicles, with the number of Pgp molecules per NIH-MDR1-G185 cell determined previously as n = 1.95 × 10^6 Pgp/cell (*8*). This yields (9.2 ± 1.5) × 10^6 P_i/cell/s. For comparison the ECAR data obtained for intact NIH-MDR-G185 and NIH3T3 cells under different metabolic conditions are summarized in Table 1. The best agreement is found for cells with high passage numbers (pn = 4−20) in the presence of glucose. The excellent correlation between ECAR data and data from ATP hydrolysis suggests that ATP synthesis is kinetically linked to ATP hydrolysis.

Previous data from Pgp reconstituted into lipid vesicles are in the range of 10^6 to 10^7 P_i/cell/s (*8*, *15*, *58*, *59*). This variation in ATP hydrolysis data is due to the fact that many experimental steps are involved in Pgp purification and reconstitution into lipid membranes and that the lipid chosen for reconstitution plays a role (*60*). After careful standardization, the error range for ECARs under a given condition is

generally relatively small. ECAR measurements have moreover the advantage of giving an *in situ* determination of Pgp activation.

Conclusions. (i) Wild-type cells showed on average 30 ± 10% higher basal ECARs than genetically modified cells such as *MDR1*- and *MRP1*- transfected cells and *Mdr1a*$^{-/-}$*1b*$^{-/-}$ knockout cells at least if measured at low passage numbers (pn = 2−3). The difference between the basal ECAR of wild-type and genetically modified cells was smallest for NIH-MDR1-G185 cells and almost vanished for cells of higher passage numbers (pn > 4). Although *MDR1*-transfected cells consume ATP at a high basal rate (perhaps due to an endogenous substrate), their basal ECARs were not higher than those of wild-type cells. Moreover, an increase in Pgp expression did not lead to an increase in basal ECARs. We thus conclude that a genetic modification, whether it is a *MDR1* or *MRP1* transfection or a *Mdr1a*$^{-/-}$*1b*$^{-/-}$ knockout, tends to reduce the basal cellular metabolism. (ii) Stimulation of *MDR1*-transfected cells by verapamil (6−10 μM) induced an increase in metabolic rates which was proportional to the expression level of Pgp, whereas stimulation of wild-type, MRP1-transfected, or knockout cells gave no response. A comparison of *MDR1*-transfected cells of low and high passage numbers (exhibiting low and high basal metabolic rates, respectively) shows that the rate of Pgp activation and the concomitant protection of cells against drugs or toxins are proportional to the basal metabolic rate of the cell. In glucose-deficient (or pyruvate-fed) NIH-MDR1-G185 cells the energy spent on detoxification by Pgp *relative* to basal values is, however, 2-fold higher than in glucose-fed cells, suggesting that the energy required to drive Pgp can be derived from endogenous energy stores under conditions of starvation. Cells overexpressing Pgp thus seem to have an efficient mechanism of self-protection against toxic compounds even under starvation conditions and consequent low basal metabolic rates. (iii) ATP is generated mainly by glycolysis, producing one molecule of lactate per ATP molecule synthesized, whereby lactate seems to be exported mainly by monocarboxylate transporters. (iv) The excellent correlation between the number of protons or lactate molecules excreted per second per cell under optimal conditions (i.e., for cells with high passage numbers in glucose-containing buffer) and the number of ATP molecules hydrolyzed by Pgp in inside-out vesicles of the same cells suggests that ATP synthesis is kinetically linked to ATP hydrolysis.

REFERENCES

1. Ambudkar, S. V., Dey, S., Hrycyna, C. A., Ramachandra, M., Pastan, I., and Gottesman, M. M. (1999) Biochemical, cellular, and pharmacological aspects of the multidrug transporter, *Annu. Rev. Pharmacol. Toxicol. 39*, 361−398.
2. Stein, W. D. (1997) Kinetics of the multidrug transporter (P-glycoprotein) and its reversal, *Physiol. Rev. 77*, 545−590.
3. Seelig, A., and Gatlik-Landwojtowicz, E. (2004) Inhibitors of multidrug efflux transporters—their membrane and protein interactions, *Mini-Rev. Med. Chem.* (in press).
4. Urbatsch, I. L., Tyndall, G. A., Tombline, G., and Senior, A. E. (2003) P-glycoprotein catalytic mechanism. Studies of the ADP-vanadate inhibited state, *J. Biol. Chem. 2*, 2.
5. Eytan, G. D., Regev, R., Oren, G., and Assaraf, Y. G. (1996) The role of passive transbilayer drug movement in multidrug resistance and its modulation, *J. Biol. Chem. 271*, 12897−12902.
6. Shapiro, A. B., and Ling, V. (1998) Stoichiometry of coupling of rhodamine 123 transport to ATP hydrolysis by P-glycoprotein, *Eur. J. Biochem. 254*, 189−193.
7. Sauna, Z. E., and Ambudkar, S. V. (2001) Characterization of the catalytic cycle of ATP hydrolysis by human P-glycoprotein. The two ATP hydrolysis events in a single catalytic cycle are kinetically similar but affect different functional outcomes, *J. Biol. Chem. 276*, 11653−11661.
8. Ambudkar, S. V., Cardarelli, C. O., Pashinsky, I., and Stein, W. D. (1997) Relation between the turnover number for vinblastine transport and for vinblastine-stimulated ATP hydrolysis by human P-glycoprotein, *J. Biol. Chem. 272*, 21160−22166.
9. Litman, T., Zeuthen, T., Skovsgaard, T., and Stein, W. D. (1997) Structure−activity relationships of P-glycoprotein interacting drugs: kinetic characterization of their effects on ATPase activity, *Biochim. Biophys. Acta 1361*, 159−168.
10. Kerr, K. M., Sauna, Z. E., and Ambudkar, S. V. (2001) Correlation between steady-state ATP hydrolysis and vanadate-induced ADP trapping in Human P-glycoprotein. Evidence for ADP release as the rate-limiting step in the catalytic cycle and its modulation by substrates, *J. Biol. Chem. 276*, 8657−8664.
11. al-Shawi, M. K., and Senior, A. E. (1993) Characterization of the adenosine triphosphatase activity of Chinese hamster P-glycoprotein, *J. Biol. Chem. 268*, 4197−4206.
12. Ramachandra, M., Ambudkar, S. V., Chen, D., Hrycyna, C. A., Dey, S., Gottesman, M. M., and Pastan, I. (1998) Human P-glycoprotein exhibits reduced affinity for substrates during a catalytic transition state, *Biochemistry 37*, 5010−5019.
13. Sharom, F. J., Yu, X., Lu, P., Liu, R., Chu, J. W., Szabo, K., Muller, M., Hose, C. D., Monks, A., Varadi, A., Seprodi, J., and Sarkadi, B. (1999) Interaction of the P-glycoprotein multidrug transporter (MDR1) with high affinity peptide chemosensitizers in isolated membranes, reconstituted systems, and intact cells, *Biochem. Pharmacol. 58*, 571−586.
14. Raggers, R. J., Pomorski, T., Holthuis, J. C., Kalin, N., and van Meer, G. (2000) Lipid traffic: the ABC of transbilayer movement, *Traffic 1*, 226−234.
15. Romsicki, Y., and Sharom, F. J. (2001) Phospholipid flippase activity of the reconstituted P-glycoprotein multidrug transporter, *Biochemistry 40*, 6937−6947.
16. Krupka, R. M. (1999) Uncoupled active transport mechanisms accounting for low selectivity in multidrug carriers: P-glycoprotein and SMR antiporters, *J. Membr. Biol. 172*, 129−143.
17. Al-Shawi, M. K., Polar, M. K., Omote, H., and Figler, R. A. (2003) Transition state analysis of the coupling of drug transport to ATP hydrolysis by P-glycoprotein, *J. Biol. Chem. 278*, 52629−52640.
18. Garrigues, A., Nugier, J., Orlowski, S., and Ezan, E. (2002) A high-throughput screening microplate test for the interaction of drugs with P-glycoprotein, *Anal. Biochem. 305*, 106−114.
19. McConnell, H. M., Owicki, J. C., Parce, J. W., Miller, D. L., Baxter, G. T., Wada, H. G., and Pitchford, S. (1992) The cytosensor microphysiometer: biological applications of silicon technology, *Science 257*, 1906−1912.
20. Landwojtowicz, E., Nervi, P., and Seelig, A. (2002) Real-time monitoring of p-glycoprotein activation in living cells, *Biochemistry 41*, 8050−8057.
21. Goda, K., Balkay, L., Marian, T., Tron, L., Aszalos, A., and Szabo, G., Jr. (1996) Intracellular pH does not affect drug extrusion by P-glycoprotein, *J. Photochem. Photobiol., B 34*, 177−182.
22. Broxterman, H. J., Pinedo, H. M., Kuiper, C. M., Schuurhuis, G. J., and Lankelma, J. (1989) Glycolysis in P-glycoprotein-overexpressing human tumor cell lines. Effects of resistance-modifying agents, *FEBS Lett. 247*, 405−410.
23. Altenberg, G. A., Young, G., Horton, J. K., Glass, D., Belli, J. A., and Reuss, L. (1993) Changes in intra- or extracellular pH do not mediate P-glycoprotein-dependent multidrug resistance, *Proc. Natl. Acad. Sci. U.S.A. 90*, 9735−9738.
24. Owicki, J. C., and Parce, J. W. (1992) Biosensors based on the energy metabolism of living cells: the physical chemistry and cell biology of extracellular acidification, *Biosens. Bioelectron. 7*, 255−272.
25. Keizer, H. G., and Joenje, H. (1989) Increased cytosolic pH in multidrug-resistant human lung tumor cells: effect of verapamil, *J. Natl. Cancer Inst. 81*, 706−709.
26. Thiebaut, F., Currier, S. J., Whitaker, J., Haugland, R. P., Gottesman, M. M., Pastan, I., and Willingham, M. C. (1990) Activity of the multidrug transporter results in alkalinization of the cytosol: measurement of cytosolic pH by microinjection of a pH-sensitive dye, *J. Histochem. Cytochem. 38*, 685−690.

27. Roepe, P. D. (1992) Analysis of the steady-state and initial rate of doxorubicin efflux from a series of multidrug-resistant cells expressing different levels of P-glycoprotein, *Biochemistry 31*, 12555−12564.
28. Boscoboinik, D., Gupta, R. S., and Epand, R. M. (1990) Investigation of the relationship between altered intracellular pH and multidrug resistance in mammalian cells, *Br. J. Cancer 61*, 568−572.
29. Hoffman, M. M., Wei, L. Y., and Roepe, P. D. (1996) Are altered pHi and membrane potential in hu MDR 1 transfectants sufficient to cause MDR protein-mediated multidrug resistance? *J. Gen. Physiol. 108*, 295−313.
30. Simon, S., Roy, D., and Schindler, M. (1994) Intracellular pH and the control of multidrug resistance, *Proc. Natl. Acad. Sci. U.S.A. 91*, 1128−1132.
31. Chen, Y., and Simon, S. M. (2000) In situ biochemical demonstration that P-glycoprotein is a drug efflux pump with broad specificity, *J. Cell Biol. 148*, 863−870.
32. Litman, T., Pedersen, S. F., Kramhoft, B., Skovsgaard, T., and Hoffmann, E. K. (1998) pH regulation in sensitive and multidrug resistant Ehrlich ascites tumor cells, *Cell Physiol. Biochem. 8*, 138−150.
33. Porcelli, A. M., Scotlandi, K., Strammiello, R., Gislimberti, G., Baldini, N., and Rugolo, M. (2002) Intracellular pH regulation in U-2 OS human osteosarcoma cells transfected with P-glycoprotein, *Biochim. Biophys. Acta 1542*, 125−138.
34. Marbeuf-Gueye, C., Priebe, W., and Garnier-Suillerot, A. (2000) Multidrug resistance protein functionality: no effect of intracellular or extracellular pH changes, *Biochem. Pharmacol. 60*, 1485−1489.
35. Schinkel, A. H., Wagenaar, E., van Deemter, L., Mol, C. A., and Borst, P. (1995) Absence of the mdr1a P-Glycoprotein in mice affects tissue distribution and pharmacokinetics of dexamethasone, digoxin, and cyclosporin A, *J. Clin. Invest. 96*, 1698−1705.
36. Cardarelli, C. O., Aksentijevich, I., Pastan, I., and Gottesman, M. M. (1995) Differential effects of P-glycoprotein inhibitors on NIH3T3 cells transfected with wild-type (G185) or mutant (V185) multidrug transporters, *Cancer Res. 55*, 1086−1091.
37. Evers, R., Zaman, G. J., van Deemter, L., Jansen, H., Calafat, J., Oomen, L. C., Oude Elferink, R. P., Borst, P., and Schinkel, A. H. (1996) Basolateral localization and export activity of the human multidrug resistance-associated protein in polarized pig kidney cells, *J. Clin. Invest. 97*, 1211−1218.
38. Allen, J. D., Brinkhuis, R. F., van Deemter, L., Wijnholds, J., and Schinkel, A. H. (2000) Extensive contribution of the multidrug transporters P-glycoprotein and Mrp1 to basal drug resistance, *Cancer Res. 60*, 5761−5766.
39. Parce, J. W., Owicki, J. C., Kercso, K. M., Sigal, G. B., Wada, H. G., Muir, V. C., Bousse, L. J., Ross, K. L., Sikic, B. I., and McConnell, H. M. (1989) Detection of cell-affecting agents with a silicon biosensor, *Science 246*, 243−247.
40. CIBA-GEIGY. (1979) *Wissenschaftliche Tabellen Geigy*, p 331, CIBA-GEIGY AG, Basel.
41. Wiley, C., and Beeson, C. (2002) Continuous measurement of glucose utilization in heart myoblasts, *Anal. Biochem. 304*, 139−146.
42. Ambudkar, S. V. (1998) Drug-stimulatable ATPase activity in crude membranes of human MDR1-transfected mammalian cells, *Methods Enzymol. 292*, 504−514.
43. Decorti, G., Rosati, A., Candussio, L., Giraldi, T., and Bartoli Klugmann, F. (2001) Characterization of multidrug transporters in a normal renal tubular cell line resistant to doxorubicin. Multidrug transporters in the LLC− PK(1) cell line and its resistant counterpart, *Biochem. Pharmacol. 61*, 61−66.
44. Restrepo, D., Cronise, B. L., Snyder, R. B., Spinelli, L. J., and Knauf, P. A. (1991) Kinetics of DIDS inhibition of HL-60 cell anion exchange rules out ping-pong model with slippage, *Am. J. Physiol. 260*, C535−C544.
45. Jackson, V. N., and Halestrap, A. P. (1996) The kinetics, substrate, and inhibitor specificity of the monocarboxylate (lactate) transporter of rat liver cells determined using the fluorescent intracellular pH indicator, 2′,7′-bis(carboxyethyl)-5(6)-carboxyfluorescein, *J. Biol. Chem. 271*, 861−868.
46. Sarkadi, B., Price, E. M., Boucher, R. C., Germann, U. A., and Scarborough, G. A. (1992) Expression of the human multidrug resistance cDNA in insect cells generates a high activity drug-stimulated membrane ATPase, *J. Biol. Chem. 267*, 4854−4858.
47. Ramachandra, M., Ambudkar, S. V., Gottesman, M. M., Pastan, I., and Hrycyna, C. A. (1996) Functional characterization of a glycine 185-to-valine substitution in human P-glycoprotein by using a vaccinia-based transient expression system, *Mol. Biol. Cell 7*, 1485−1498.
48. Hewitt, C. O., Eszes, C. M., Sessions, R. B., Moreton, K. M., Dafforn, T. R., Takei, J., Dempsey, C. E., Clarke, A. R., and Holbrook, J. J. (1999) A general method for relieving substrate inhibition in lactate dehydrogenases, *Protein Eng. 12*, 491−496.
49. Pelster, B., and Niederstatter, H. (1997) pH-dependent proton secretion in cultured swim bladder gas gland cells, *Am. J. Physiol. 273*, R1719−R1725.
50. Miller, D. L., Olson, J. C., Parce, J. W., and Owicki, J. C. (1993) Cholinergic stimulation of the Na+/K+ adenosine triphosphatase as revealed by microphysiometry, *Biophys. J. 64*, 813−823.
51. Hamilton, G., Cosentini, E. P., Teleky, B., Koperna, T., Zacheri, J., Riegler, M., Feil, W., Schiessel, R., and Wenzi, E. (1993) The multidrug-resistance modifiers verapamil, cyclosporine A and tamoxifen induce an intracellular acidification in colon carcinoma cell lines in vitro, *Anticancer Res. 13*, 2059−2063.
52. Dimmer, K. S., Friedrich, B., Lang, F., Deitmer, J. W., and Broer, S. (2000) The low-affinity monocarboxylate transporter MCT4 is adapted to the export of lactate in highly glycolytic cells, *Biochem. J. 350 Pt 1*, 219−227.
53. Wilson, M. C., Jackson, V. N., Heddle, C., Price, N. T., Pilegaard, H., Juel, C., Bonen, A., Montgomery, I., Hutter, O. F., and Halestrap, A. P. (1998) Lactic acid efflux from white skeletal muscle is catalyzed by the monocarboxylate transporter isoform MCT3, *J. Biol. Chem. 273*, 15920−15926.
54. Tse, C. M., and Young, J. D. (1990) Glucose transport in fish erythrocytes: variable cytochalasin-B-sensitive hexose transport activity in the common eel (Anguilla japonica) and transport deficiency in the paddyfield eel (Monopterus albus) and rainbow trout (Salmo gairdneri), *J. Exp. Biol. 148*, 367−383.
55. Krupka, R. M. (1985) Asymmetrical binding of phloretin to the glucose transport system of human erythrocytes, *J. Membr. Biol. 83*, 71−80.
56. Schmid, D., Ecker, G., Kopp, S., Hitzler, M., and Chiba, P. (1999) Structure−activity relationship studies of propafenone analogs based on P-glycoprotein ATPase activity measurements, *Biochem. Pharmacol. 58*, 1447−1456.
57. Venter, H., Shilling, R. A., Velamakanni, S., Balakrishnan, L., and Van Veen, H. W. (2003) An ABC transporter with a secondary-active multidrug translocator domain, *Nature 426*, 866−870.
58. Shapiro, A. B., and Ling, V. (1994) ATPase activity of purified and reconstituted P-glycoprotein from Chinese hamster ovary cells, *J. Biol. Chem. 269*, 3745−3754.
59. Urbatsch, I. L., al-Shawi, M. K., and Senior, A. E. (1994) Characterization of the ATPase activity of purified Chinese hamster P-glycoprotein, *Biochemistry 33*, 7069−7076.
60. Romsicki, Y., and Sharom, F. J. (1999) The membrane lipid environment modulates drug interactions with the P-glycoprotein multidrug transporter, *Biochemistry 38*, 6887−6896.

BI048761S